Detection of Breaking Events in a Wind-Generated Wave Field[1]

M. A. WEISSMAN,[2] S. S. ATAKTÜRK AND K. B. KATSAROS

Department of Atmospheric Sciences, University of Washington, Seattle, WA 98195

(Manuscript received 6 October 1983, in final form 26 June 1984)

ABSTRACT

Measurements were made of the surface elevation of a fetch-limited wave field (fetch 7 km, wind speed about 6 m s^{-1}). Good high-frequency response was attained by the use of a very thin, bare wire probe of diameter 0.13 mm. Breaking waves were detected based on the energy in the 18–32 Hz frequency band. An appropriate threshold was found by a trial and error method. General agreement was found with visual observations.

The temporal intermittency of wave breaking (fraction of time spent in breaking regions) was found to be only 1.2%; however, the fraction of high-frequency (5–50 Hz) energy in those regions was 12%. An argument is presented to show that the spatial intermittency and the spatial energy fraction should have the same values.

The mean crest height of the breaking waves was found to be much lower than expected from theoretical considerations (by a factor of 4).

1. Introduction

This study was simulated by an investigation of acoustic scattering from the air–water interface from below (McConnell *et al.*, 1984). As in the analogous case of electromagnetic radiation from above, scattering is mainly due to the small-scale structure of the surface, through the mechanisms of Bragg scattering and corner reflections (Wright, 1966).

Although empirical studies have been made relating backscatter intensity to wind speed and other environmental conditions (Krishen, 1971; Jones and Schroeder, 1977), relatively little is known about the direct correlation of the return to the character of the scattering medium itself, that is, to the spatial structure of the surface on scales of 0.1 to 30 cm. Thus, some key questions of importance for further modeling of the process remain unanswered. For example, is the scattering mainly due to short surface waves, which are generally present due to their continual generation by the wind, or is a large fraction of the scattering due to wave breaking events, which are only present intermittently but are so energetic that they may provide the greater part of the scattering cross section?

To answer this question requires intensive, small-scale, spatial measurements of the sea surface in conjunction with radar or acoustic observations. This capability is not yet available; however, intensive, high-frequency, temporal measurements can be made. The present study uses these types of observations to address the question of how important breaking events are likely to be. Our approach is to define and then detect the events in the time series of surface elevation. Then by conditional averaging, we can determine to what degree breaking events "stand out" above the normal background and how much they contribute to the total energy.

The energy of interest to backscattering we will consider to be in the 5–50 Hz frequency band. These frequencies are related to the spatial band of interest, 0.1 to 30 cm, but there is no direct connection. The frequency of a surface component of, say, 1.7 cm length depends on the speed and direction that it passes by the probe. If there are no currents and if this component is a gravity–capillary wave, its frequency would be about 13.5 Hz (and its phase speed would be 23 cm s^{-1}). However, if it is riding in a current of 50 cm s^{-1}, which is typical of the orbital velocity of long waves, its observed frequency would be 43 Hz. On the other hand, this component might not be a gravity–capillary wave at all. It could be part of the turbulent structure that accompanies a breaking wave, and its frequency would be determined by the speed that the turbulent patch moves past the probe (usually the phase speed of the breaking waves).

Thus, there are two main problems in any attempt to relate temporal measurements of the small-scale surface structure to spatial quantities: 1) the small-scale structure may be due to either waves or turbulence, and 2) the relation between frequency and wavelength is a strong function of the local currents and, in particular, of the orbital velocities of longer waves.

[1] Dept. of Atmospheric Sciences, University of Washington, Contribution Number 713.

[2] Present affiliation: Microscience, Inc., Federal Way, Washington 98003.

To a certain extent, the second problem can be resolved by applying the Doppler shift formula:

$$\omega = \sigma + Uk\cos\theta, \tag{1.1}$$

where ω is the measured frequency, σ the intrinsic frequency (the frequency that the component would have in still water), U the current (mean plus long wave orbital motions), k the wavenumber magnitude of the component under consideration, and θ is the angle between the wave direction and the current direction. Thus, in theory, by measuring $\omega(t)$, $U(t)$, and $\theta(t)$ and by assuming a dispersion relation, $\sigma(k)$, we could apply (1.1) and determine $k(t)$. This approach has been used, in varying ways, by several investigators (Sinitsyn *et al.*, 1973; Reece, 1978; Stolte, 1979; Evans and Shemdin, 1980; Richter and Rosenthal, 1981).

In practice, however, it is very difficult to measure $U(t)$ and $\theta(t)$ directly, and it is not obvious what to use for $\sigma(k)$. Even if we are confident that we are measuring gravity–capillary waves, they are undergoing active generation by the wind and $\sigma(k)$ can be expected to be a function of the local turbulent boundary layer structure.[3] At times the component ω will be part of a turbulent "burst," a breaking event. Then $\sigma(k)$ should be set to zero by Taylor's hypothesis (Kraus, 1972). Another problem in the application of (1.1) for gravity–capillary waves was elucidated by Phillips (1980): The relationship between ω and σ (or k) can be multivalued. For a given measurement of ω, there can be two values of σ.

Given these uncertainties in any attempt to apply the Doppler shift correction, the present report concentrates on the first problem mentioned above: To what extent is the energy in the high frequency part of the spectrum influenced by, or even dominated by, breaking events? (Further work in our research program will address the second problem.) The data used are wind and wave measurements made at the University of Washington's MSMAST site in Lake Washington. The experimental apparatus and the data sets are described in Section 2.

Section 3 describes the preliminary processing algorithm, which separated the "long" waves from the "short" waves. This resulted in time series for the elevation of the long waves and for the energy spectrum of the short waves. A "breaking wave detector" was designed based on the increase in energy in a high-frequency band and the simultaneous presence of a wave crest. This algorithm is described in Section 4 and the results in Section 5. Section 6 shows how these temporal results can be converted to spatial quantities.

In Section 7, we examine how the elevation of the breaking wave crests compare to the theories of Longuet-Higgins (1975) and Banner and Phillips (1974). We found that the measured elevation of the breaking crests was much lower than predicted. Possible implications of this are discussed in Section 8, along with a summary of the main results and comparisons to other work.

2. Experimental site and instrumentation

The field measurements for this study were made during July 1982 on Lake Washington at the MSMAST facility operated by the University of Washington, Department of Atmospheric Sciences. The facility consists of various environmental instruments mounted on a mast located about 20 m offshore in a water depth of approximately 4 m. (Since the peak wavelength of the waves we were observing was about 5 m. (Table 1), this can be considered to be "deep water.") Ideal experimental conditions are achieved during northerly winds when the fetch reaches its maximum of about 7 km, see Fig. 1. The environmental conditions during the study are summarized in Table 1.

Figure 2 shows the data paths for the data acquisition and analysis. The water surface elevation was measured by a resistance wire gauge consisting of a stainless steel wire, 0.13 mm diameter, hung vertically from the mast and a ground plate placed on the lake bottom. The resistance of the portion of the wire exposed to the air is a linear function of the water surface elevation, to a very good approximation. In order to avoid the dynamic range limitations of the recording unit, the output signal was recorded in two channels: the low-pass channel, which was the original signal low-pass filtered at 50 Hz (half-amplitude point), and the high-pass channel, which was obtained from the low-pass signal by sending it through a 5 Hz high-pass filter (see Fig. 2). The 50 Hz filter was chosen to reduce 60 Hz noise. The filter characteristics are shown in Fig. 3.

Prior to the field measurements, the dynamic performance of the wave probe was tested against a laser displacement gauge (LDG) in a wind-wave tank (Liu *et al.*, 1982). Comparisons between the two systems showed that, in the frequency range 10 to 40 Hz, the spectral densities obtained from the wire gauge were consistently lower than those from the LDG by 30 to 45%. In that report, agreement between the two

[3] Assuming thin layers of constant shear on both sides of the interface, Weissman (1976) has shown that Kelvin's (1871) result is appropriate:

$$\sigma = \hat{\rho}\hat{U}k + (\sigma_0^2 - \hat{\rho}\hat{U}^2k^2)^{1/2},$$

where $\hat{\rho}$ is the density ratio (=0.00125), σ_0 is the frequency without currents, and $\hat{U}$ is the velocity difference between air and water measured just outside the shear layers. (A similar result was reached by Miles, 1957.) For a turbulent boundary layer, these shear layers can be interpreted as the viscous sublayers. As a consequence $\hat{U}$ is 10 or 11 times the friction velocity u^* (Schlichting, 1968). Hence, σ will be sensitive to u^*, which can be expected to vary along the phase of the long waves.

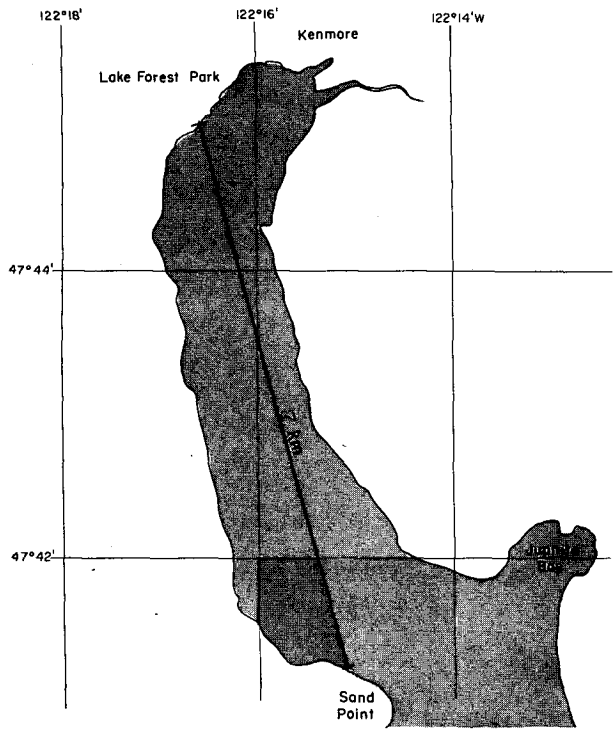

FIG. 1. Location of the experimental site.

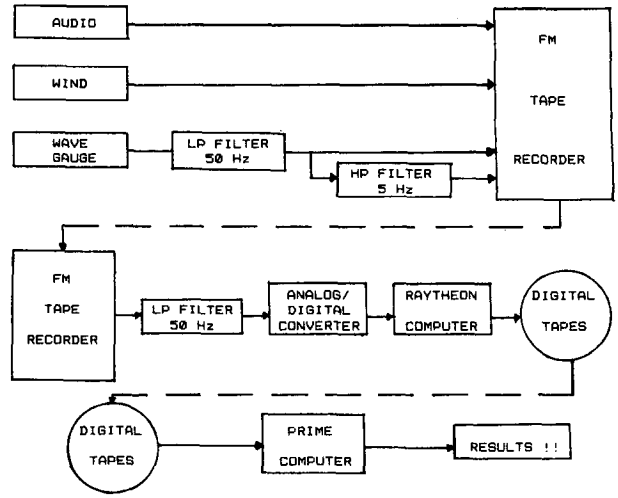

FIG. 2. Data paths.

methods was achieved after an empirical correction was applied to the wire gauge data. In the present study we are only interested in relative energy levels; therefore the correction has not been applied.

Preliminary spectra (Fig. 4) were computed on a Raytheon 704 computer before the data were passed on to a Prime 400 for further processing (see Fig. 2). For convenience and to eliminate bad patches, the total run of about 10 minutes was separated into three data segments (see Table 1). The composite spectra in Fig. 4 is a superposition of the two separate spectra from the low-pass and high-pass channels. Self-consistency is confirmed by the excellent match in the region of 6–10 Hz. Beyond 10 Hz the low-pass signal is lost within the noise of the recording system (which includes 60 Hz fundamental and subharmonics). No corrections have been applied for filter response or dynamic response of the wire.

Wind speed and direction were measured by a Gill anemometer. This system consisted of two propellers, one aligned horizontally and the other inclined from the horizontal, making it possible to calculate vertical velocities (Pond and Large, 1978). A vane keeps the propellers aligned into the wind. The speed of both propellers was recorded, but only the horizontal component has been used in the present study. (Stress measurements are available for future studies.) The anemometer was calibrated in a wind tunnel at the Department of Atmospheric Sciences before the experiment.

The horizontal wind speed and the two channels of wave data were recorded on an Ampex SP700 FM tape recorder capable of recording frequencies up to 2500 Hz. A fourth channel was used for observer

TABLE 1. Experimental conditions.

	Data segment			Total
	767-1	767-2	767-3	run
Duration (s)	128.50	256.50	256.50	641.50
Wind speed (m s^{-1})	5.34	5.90	6.18	5.90
Air-water temperature difference (°C)	—	—	—	−0.04
Dominant wave:				
Frequency (Hz)	0.57	0.55	0.56	0.56
Wavelength (m)	4.80	5.16	4.97	5.01
rms wave amplitude (cm)	4.28	4.31	4.01	4.18

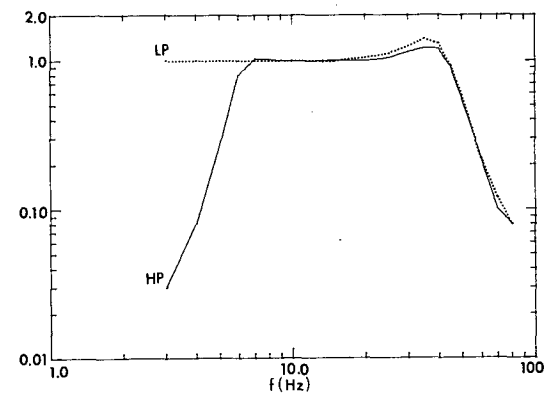

FIG. 3. Filter characteristics of the wave gauge. LP: low-pass filter at 50 Hz; HP: additional high-pass filter at 5 Hz.

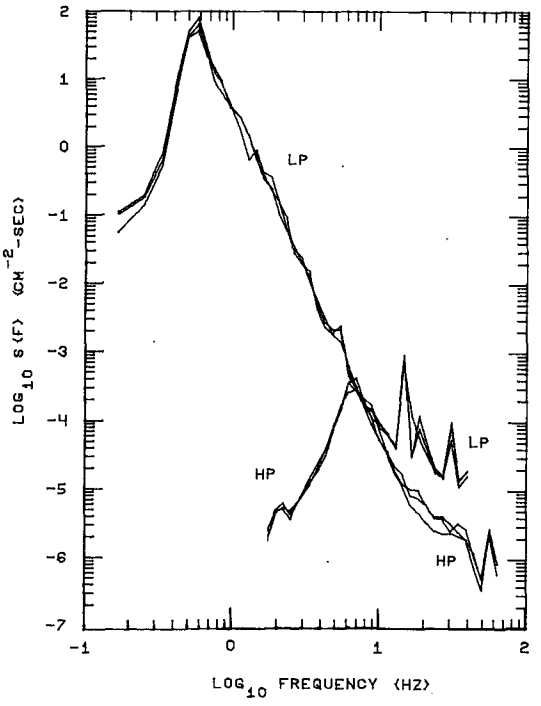

FIG. 4. Composite spectra of the LP and the HP channels. (All three data segments are plotted.)

commentary. Other parameters (the other wind components, the wind direction, wet- and dry-bulb temperatures, water temperatures, radiation, etc.) were recorded at the same time on another tape system, but they are not pertinent to the present study.

During the period of data acquisition, visual and audio records were also made. Close-up photographs (35 mm slides) were taken of the water surface to record the small-scale structure. A Nikon F-2 camera was mounted on the mast and focused on the spot where the wire penetrated the surface. The camera could be triggered remotely from shore. Figure 5 shows examples of these photographs. On the audio channel of the tape recorder, a description of the water surface was recorded. Breaking events and the exposure of a photograph were especially noted.

The analog data on tape were then converted into computer compatible records on the Raytheon 704 using a 12-bit analog-to-digital converter which digitized each channel at a rate of 256 points per second. The data were then recorded on digital tape and transferred to the Prime 400 with which the major part of the data analysis was performed.

3. Preliminary processing

The first stage of the data analysis on the Prime computer was to compute the wave elevation due to the low-frequency part of the wave signal and the spectral energies of the high-frequency part. This was achieved by calculating a "running" average of the low-pass channel and a "running" fourier transform of the high-pass channel. (This program is called RASP for "running averages and spectra".)

A window of 0.5 s length (128 points) was passed along the data. At each window position, the data were multiplied by a weighting function having a cosine shape (Hanning):

$$W(i) = [1 - \cos(2\pi i/128)]/W_0, \quad i = 0, 1, \ldots, 127, \tag{3.1}$$

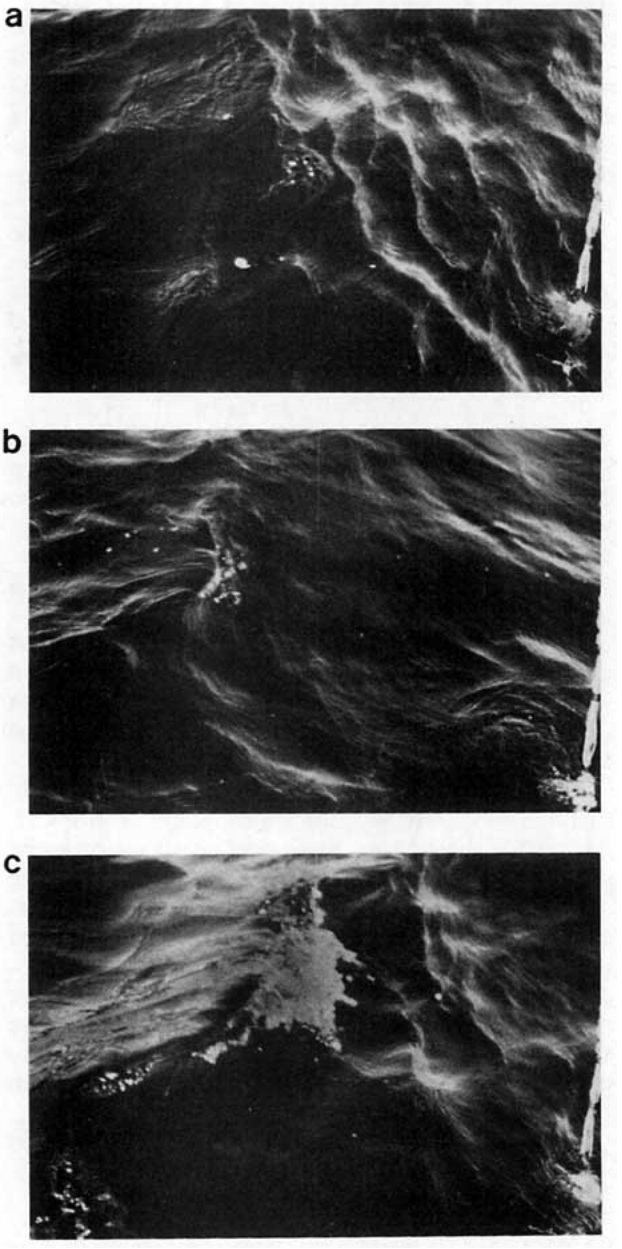

FIG. 5. Photographs of breaking events; (a) generation of a turbulent patch without air entrainment, (b) a "small-scale" breaking crest and (c) a "large-scale" breaking crest.

where

$$W_0 = \sum_{i=0}^{127} [1 - \cos(2\pi i/128)].$$

As illustrated in Fig. 6, the window is moved forward 0.125 s, or 32 points, before the next point is calculated. This results in new time series that are sampled at 8 points per second.

For the low-pass channel, the weighted mean within the window was calculated. This is equivalent to applying a low-pass filter of 2 Hz (½ amplitude point) and decimating the data at 8 Hz. The filter is symmetric; i.e., there is no phase shift.

For the high-pass channel, a fast Fourier transform was performed and the energy spectrum was calculated at every window position. This gave 64 spectral estimates every eighth of a second. The estimates were normalized to conserve variance. Note that detrending was not necessary since this channel was previously high-pass filtered.

The length of the window was a compromise between good temporal resolution (short window) and good spectral resolution (long window). The present choice gives 16 points per wave period and 23 spectral estimates in the frequency band of interest, 5–50 Hz.[4]

Figure 7 shows the raw data before the processing was done. There are "bursts" of energy in the high-passed channel, which are most likely due to breaking events (note event at about 3.5 s and its correlation with wave crest). There is also a strong event at about 6 s that is not associated with a wave crest; therefore, we do not regard this as a breaking event. It is probably due to a localized wind event, such as a cats-paw. This type of signal is relatively rare. Most often, activity in the high-pass channel is correlated with wave crests, even when wave breaking is not evident. This can be seen in Fig. 7b, which is a typical section of data without breaking events.

The results of processing with RASP are shown in Fig. 8. The first 16 seconds are the same as in Fig. 7. Except for the bottom two traces, each curve is the spectral estimate at the frequency indicated. The square root has been plotted so that extreme values could be better seen, and the curves have been scaled using approximate maximum values. Relative energies of the various frequencies are not important to the present study. The bottom curve is the long-wave elevation record, and the second curve is the total energy in the high-frequency channel (5–50 Hz, again the square root has been plotted).

Note that, on occasion, energy is increased throughout the entire high-frequency band: e.g., at 3.5, 41, and 60 s. There are also times when energy has increased only in the middle ranges. To investigate this further, sums were taken over various frequency bands (program BANDS).

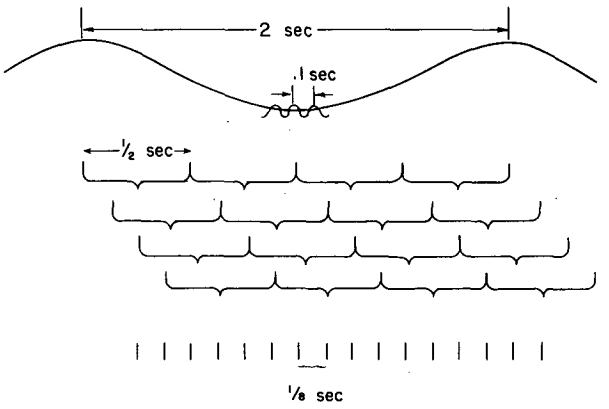

FIG. 6. The sliding window used for smoothing of the LP channel and fourier analysis of the HP channel. (Original sampling rate was 256 samples per second)

The bands were chosen as follows: In our range of interest, there is a characteristic frequency given by the balance between gravity and surface tension. This is about 13.5 Hz, which is the intrinsic frequency of gravity–capillary waves having the minimum phase speed. Therefore, the bands were chosen to relate to this frequency. Two bands split the high frequencies (6–12 and 14–32), one band is on the gravity side (6–10), one is on the capillary side (18–32), and one straddles the characteristic frequency (10–18).

The results of BANDS are illustrated in Fig. 9. There is a general difference between the traces for the midrange frequencies (6–10, 6–12, 10–18) and the high frequencies (14–32, 18–32). The total high-pass energy (the second trace up from the bottom) is very similar to the midrange bands because it is dominated by these frequencies. The bottom trace is again the long-wave elevation. There are eight or nine occasions in Fig. 9 when activity in the midrange is "supported" by activity in the high range. There are other occasions when there is only activity in the midrange. This has led us to the conclusion that the bursts of energy in the highest frequency bands are indicative of breaking events. This argument is pursued further in the next Section.

4. Design of the breaking wave detector

The rationale used in the design of the breaking wave detector was the following:

1) The results from RASP show that there are "events" when the energy is substantially increased throughout the high frequency part of the spectrum.

2) The events are presumably the result of the

[4] This process was meant to serve a few purposes; thus, it is not optimized for the detection of breaking waves. As we shall see, only the energy in the 18–32 Hz range is needed. Other methods could be devised to calculate this more efficiently.

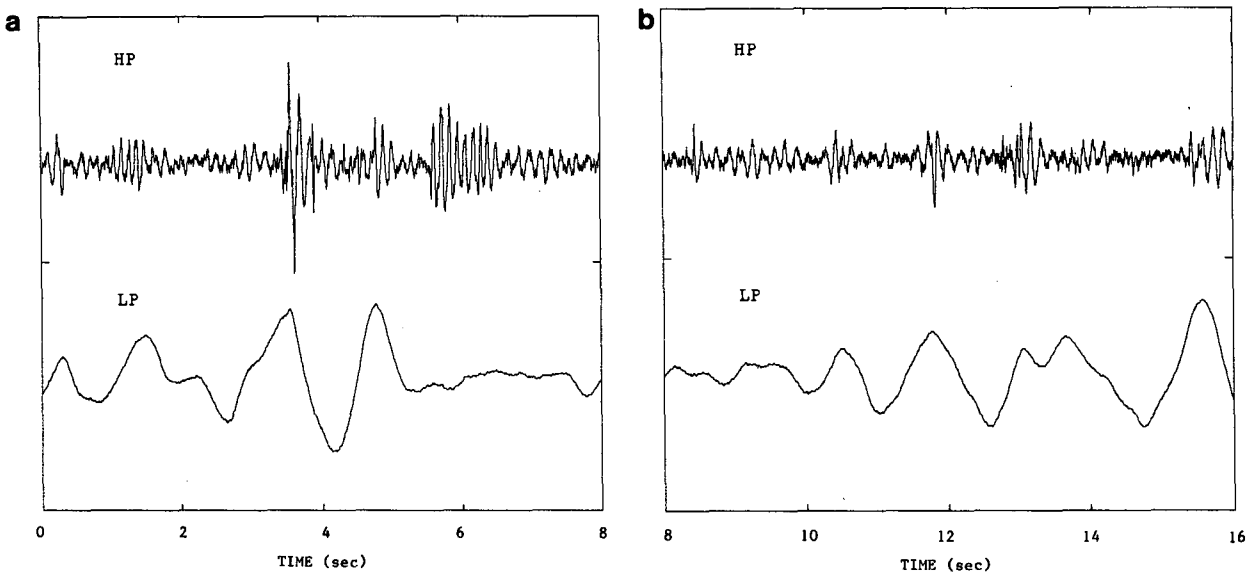

FIG. 7. Part of the original wave elevation signals from data segment 767-2: (a) 0–8 seconds, (b) 8–16 seconds.

generation of turbulence or of the appearance of a sharp corner on the surface, either of which would be associated with wave breaking.

3) The best descriminator of such an event would be the energy in the highest frequencies since the shortest scales are dissipated most rapidly. That is, these frequencies would stand out best from their background levels.

4) We expect breaking events at or near wave crests.

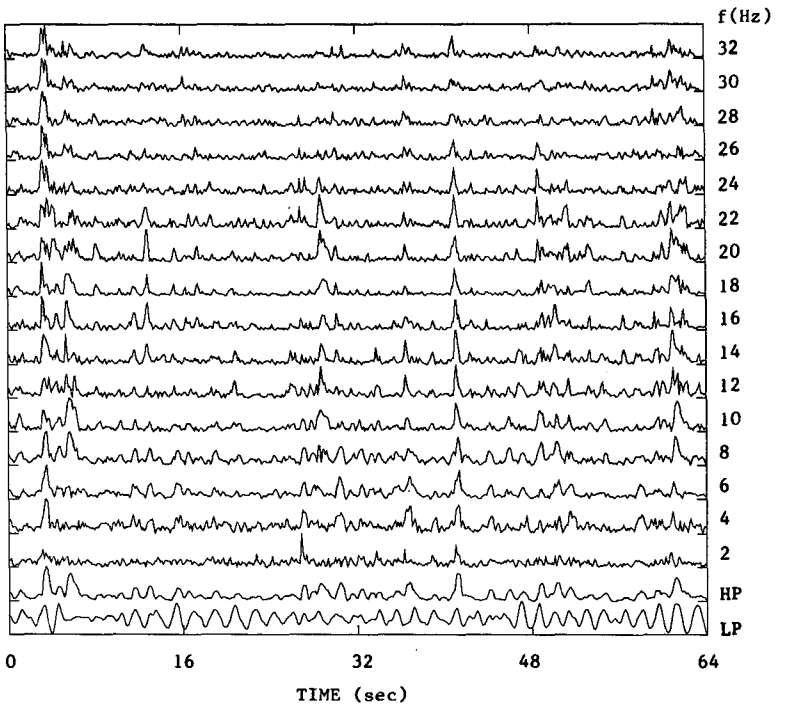

FIG. 8. Output from RASP: spectral energies for frequencies of 2–32 Hz (top 16 curves), total energy in the HP channel (second curve up from bottom), and LP elevation (bottom curve). Square root energies are plotted; vertical scales are arbitrary. From data segment 767-2, time 0–64 seconds.

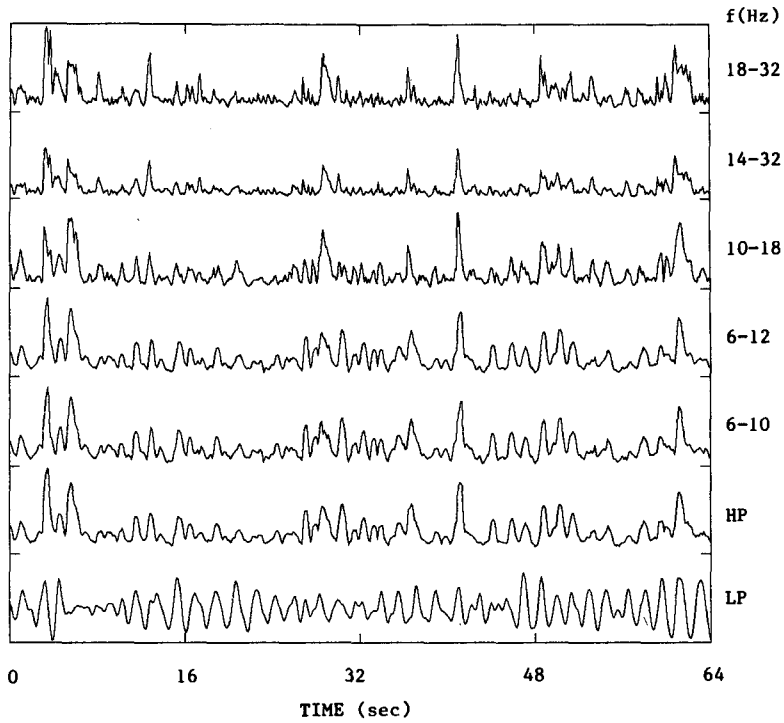

FIG. 9. Output from BANDS: spectral energies for various frequency bands (top 5 curves), total energy in the HP channel (second curve up from bottom), and LP elevation (bottom curve). Square root energies are plotted; vertical scales are arbitrary. From data segment 767-2, time 0–64 seconds.

Therefore, the detector function was chosen to be the energy (i.e., the variance of the surface elevation) in the 18–32 Hz band. The upper limit is considered to be a reasonable bound on the frequency response of the instrument (the spectra of some runs start to degenerate into noise at about this frequency). Of course, we know that the frequency response of the wire is generally low in this region (Liu *et al.*, 1982); however, our detection scheme is based on the energy in this band compared to its background value, not to an absolute value.

The detector function $D(t)$ was actually calculated as

$$D(t) = \sum_{f=18}^{32} S_f(t)\Delta f,$$

where $S_f(t)$ are the running spectral estimates from RASP and Δf is the frequency resolution (2 Hz). Thus, $D(t)$ is a time series sampled at eight points per second, and the minimum duration of an event that we can measure is 0.125 s.

After choosing a detector function, we must specify an appropriate threshold level. Two preliminary methods were ruled out: 1) to correlate breaking events, and thus threshold levels, with visual observation, and 2) to fix the threshold as some fraction of the mean value (e.g., Khalsa and Businger, 1977, in a study of intermittency in atmospheric convective boundary layers take the threshold to be equal to the mean value). For the former method, it was difficult to see and record precisely what was happening at the probe. For the latter method, we could not find any intrinsic argument for what this fraction might be. It is probably a function of conditions during a run, as is the threshold itself.

The method finally used was based on the fundamental assumption that, if it is possible to separate "events" from "background," then the statistical properties of these two modes of behavior must be sufficiently different. In particular, we expect that the probability density function for all the data should be a combination of two distributions, one for the events and one for the background. If the correct detector function is chosen, the total distribution should have two modes, between which lies the optimum choice for a threshold. Equivalently, the cumulative probability function should have a plateau.

Thus, ultimately the method used was to look for such a plateau in a suitable cumulative distribution. Figure 10 shows the results of using variable threshold levels in determining the number of breaking events. (The criteria of being near a wave crest was also used here, see below.) For each data segment and for the entire run, relatively flat regions were found at the

same values of the threshold. This region therefore contains the best value for the threshold for these experimental conditions. It was chosen to be 7.25 $\times 10^{-4}$ cm^2, the midpoint of the region indicated by the double-arrow in Fig. 10.

A breaking event will have one or more points for which the detector function is above the threshold, but, in addition, these points should lie on or near a crest of the underlying long wave (otherwise, the high-frequency activity might be due to other causes, such as cats-paws). The crest point itself was defined to be a local maximum in the long-wave elevation record, and one-eighth of a wave period was considered to be a reasonable definition of a crest "region" (i.e., ±0.125 s, or one time step, around the crest point).

Therefore, the full definition of a "breaking event" was

1) There is a (contiguous) group of one or more points where the detector function is above the threshold, and

2) One or more of these points are within ±0.125 s of a local maximum of the long-wave elevation.

5. Results of the breaking detection

For each point in the time series, the detector function was tested to see if it was above the threshold, and the long-wave elevation was tested to see if it was at or near a local maximum. A number of categories were specified, such as: all points, all points above the threshold, all points at a crest (i.e., at a local maximum). For each category, basic statistics were calculated: the number of points, the average long-wave elevation, the variance in the 18–32 Hz band (i.e., the mean of the detector function), the variance in the entire high-frequency band and the mean wind speed.

The two categories we are mainly interested in comparing are 1) all points and 2) all points above the threshold and in a group that is within one time step (0.125 s) of a local maximum. The latter category is our definition for points that are in breaking events. The number of such groups (events) was also counted.

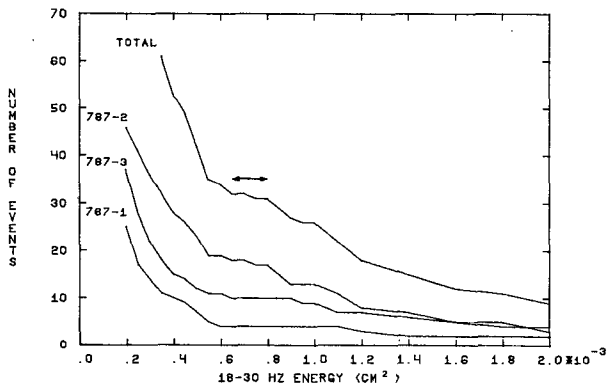

FIG. 10. The number of breaking waves detected by the algorithm as a function of the threshold assumed for the high frequency energy.

TABLE 2. Temporal statistics for breaking waves.

All points:	
Number of crests	359
Length of record	641.5 s
High-frequency variance	0.00195 cm^2 ± 0.00018
Integrated variance	1.25 cm^2 s ± 0.12
Breaking events only:	
Number of crests	31
Average length of event	0.25 s ± 0.06
High-frequency variance	0.0195 cm^2 ± 0.0043
Integrated variance	0.151 cm^2 s ± 0.07
Ratios:	
Breaking crests/total crests	8.64%
Breaking rate	2.9/min
Intermittency	1.21% ± 0.29
Fractional variance	12.1% ± 6.7

Notes:
1. The variance is for the frequency band from 5 to 50 Hz.
2. The uncertainty indicated is the sampling error at the 95% confidence level (1.96 times the standard error of the mean), except for the error in average length of the breaking events, which is half the resolution of our technique.

Table 2 summarizes the results. There were 31 breaking crests during the entire 641.5 second run. Of these, 8 were very energetic and, from rough correlation with visual observations, appeared to be large-scale spilling breakers (as in Fig. 5c). The rest were either small spilling breakers (Fig. 5b), or crests that were very "peaky" (breaking without entrainment of air, see Fig. 5a).

This number should be compared to the total number of crests. The actual number of local maxima was 506; however, this is not the best criterion to use because it includes crests due to small-scale waves. A more representative number is the number of crests that would be in the long wave alone. From the length of the run (641.5 s) and the frequency at the peak of the spectrum (0.56 Hz), this is 359. (This is also better for comparison to other experiments where the number of local maxima can not be counted.) Thus, the ratio of breaking crests to peak wave crests is about 8.6%.

The intermittency is defined as the time spent in breaking events (7.75 s, as determined from the number of points in category 2) divided by the total time of the run (641.5 s). This is only 1.2%.

However, the more important quantity for radar and sonar backscatter is the energy of the high-frequency signal (5–50 Hz) in the breaking events as compared to that in the entire run (the "fractional variance"). We found that the energy density (the variance) for the breaking events was ten times that for the entire run. Thus, even though the time spent in breaking events is about a hundredth of the total

time, the energy in those events is about a tenth of the total energy (12%, actually).

It should be remembered that these are temporal results. That is, the intermittency and fractional energy are for a probe in a fixed position. These quantities might not be directly transferrable to spatial observations, such as those made by a radar or sonar. This question is addressed in the next section.

6. Conversion of temporal results to spatial results

Since the waves do not move past the probe without change of form, it is not obvious how to interpret the temporal measurements of intermittency and fractional energy. Due to the difference between phase velocity and group velocity, wave crests move through wave packets twice as fast as the packet is moving. A crest will appear at the rear of a packet, break in the center where its amplitude is largest, and then stop breaking as it moves toward the front of the packet where it disappears. (This is illustrated in Fig. 11.) Thus, the crests measured with a stationary probe are not the same as those observed spatially, much less the breaking events themselves.

However, we can relate the wave packets, that is, the propagation of energy. Consider a line parallel to the direction of the group velocity of the dominant waves and passing through the wave gage. During an experimental run, the probe observes the wave packets (not the same peaks and troughs) that lie along this line. In order for the amount of energy observed in time to be equal to that observed in space, the length of the line must be

$$L = c_g T, \tag{6.1}$$

where c_g is the group velocity and T is the duration of the experiment.

The spatial intermittency can be defined as

$$\delta_s = \sum_{i=1}^{N_L} l_i/L, \tag{6.2}$$

or,

$$\delta_s = N_L \bar{l}/L, \tag{6.3}$$

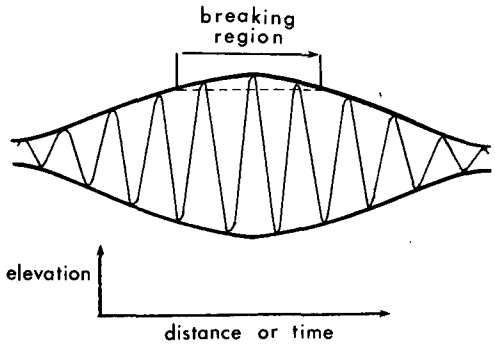

FIG. 11. Crests breaking at the center of a wave group. The dotted line is a possible amplitude threshold for breaking.

where l_i is the length of an individual breaking patch, $\bar{l}$ is the average length of a patch, and N_L is the number of breaking events in length L. (An implicit assumption is that the wave field is homogeneous in both directions and stationary in time.)

The length l_i of an individual patch can be determined from the time that it takes the patch to move past the probe position if we know the velocity with which the patch is moving. (Since the duration is typically very short, we can assume the patch is not evolving during this time.) That is,

$$l_i = (vt)_i, \tag{6.4}$$

where v is the velocity and t is the duration. Therefore, a measurement of the average patch length is

$$\bar{l} = \sum_{i=1}^{N_T} (vt)_i/N_T, \tag{6.5}$$

where N_T is the number of breaking events in time T. (Note that

$$\sum_{i=1}^{N_L} l_i \neq \sum_{i=1}^{N_T} (vt)_i;$$

the patches that lie along the line are not the same ones observed by the probe.) Substituting (6.1) and (6.5) into (6.3),

$$\delta_s = \frac{N_L \sum_{i=1}^{N_T} (vt)_i}{N_T c_g T}. \tag{6.6}$$

We do not have measurements of v, but there is good reason to take it to be equal to c, the phase speed of the dominant wave. In order for a wave crest to start breaking, the particle velocity at the crest must become equal to its propagation speed. Then the spilling part of the breaker is carried forward with the crest until the amplitude decreases and the turbulence is left behind. Thus for most of its lifetime, the turbulent patch will move with the crest velocity; at least this will provide a good upper bound. The best estimate that we have of this velocity is the phase speed of the wave at the peak of the spectrum.

Now we need to relate the number of breaking crests in L to the number in T. It is reasonable that the proportion that are breaking in L would be the same as the proportion that are breaking in T; that is

$$N_L/M_L = N_T/M_T, \tag{6.7}$$

where M_L is the number of crests in length L and M_T is the number of crests in time T. A rationale for this argument comes from the simple view of the breaking process shown in Fig. 11. Here it is assumed that a threshold exists for crest amplitude (or some other wave parameter) that determines when breaking will occur. For a typical wave packet, the length of the region where the crests exceed the threshold will be some fraction of the total length of the packet.

The proportion of breaking crests will be equal to this same fraction, which is a function of the shape of the wave packet. Therefore, if the shape of the wave packet is the same when viewed as a function of time or space, the proportion of breaking waves will also be the same.

If the evolution of the wave packet shape is slow then it will pass the probe without change of shape, and (6.7) will be correct. Most theoretical work (e.g., Lake and Yuen, 1978) assumes that envelopes evolve slowly; however, Longuet-Higgins and Cokelet (1978) have shown that there are instabilities that can lead to rapid changes of shape. We do not know which is the case in the real world, but it seems reasonable to use (6.7) as a working hypothesis for the time being.

Therefore,

$$N_L/N_T = M_L/M_T = (L/\lambda)/(Tf) = c_g/c = \frac{1}{2}, \quad (6.8)$$

where λ is the wavelength and f is the frequency of the dominant wave. Substituting $v = c$ and (6.8) into (6.6) results in

$$\delta_s = \sum_{i=0}^{N_T} t_i/T = \delta_T. \quad (6.9)$$

Thus, the two intermittencies are equal.

A similar argument shows that the spatial fractional variance (the ratio of energy in breaking events to total energy) is also the same as the temporal quantity. The inferred spatial statistics are summarized in Table 3.

TABLE 3. Inferred spatial statistics for breaking waves.

All points:	
Number of crests :	179.5
Length of record :	897.0 m ± 18.3
High-frequency variance :	0.00195 cm² ± 0.00018
Integrated variance :	1.75 cm² m ± 0.20
Breaking events only:	
Number of crests :	15.5
Average length of event :	70.0 cm ± 18.2
High-frequency variance :	0.0195 cm² ± 0.0043
Integrated variance :	0.212 cm² m ± 0.10
Ratios:	
Breaking crests/total crests :	8.64%
Breaking rate :	17/km
Intermittency :	1.21% ± 0.29
Fractional variance :	12.1% ± 6.7

Notes:
1. The variance is for the frequency band from 5 to 50 Hz.
2. The uncertainty indicated is the sampling error at the 95% confidence level (1.96 times the standard error of the mean), except for the error in average length of the breaking events, which is half the resolution of our technique.

7. Crest elevations and slopes for breaking waves

We found the somewhat surprising result that, when the waves were breaking, the wave amplitudes were much lower than expected from theoretical results. Nonlinear calculations for steady, periodic waves, such as those of Longuet-Higgins (1975), show that breaking occurs when

$$ak = 0.443,$$

where a is the amplitude and k the wavenumber. This is the overall slope parameter (a equals half the peak-to-trough distance) which should not be confused with the local slope of the interface. Our measurements of this parameter are summarized in Table 4. The value for k is obtained from the dispersion relation,

$$k = (2\pi f)^2/g = 1.26 \text{ rad/m}$$

for $g = 9.81$ m s^{-1} and $f = 0.56$ Hz, the frequency at the peak of the spectrum. For breaking crests, ak is about a quarter of the calculated value on average and even the maximum measured values are half those expected.

Another theoretical viewpoint is provided by Banner and Phillips (1974). From the basic premise that breaking will occur when the particle velocity at the surface becomes equal to the phase speed (again for a periodic wave), they show that the amplitude for breaking can be reduced considerably if a drift current is present. Their formula is

$$a = (c - q)^2/2g,$$

where q is the surface drift. Using a generous value (=0.04) for the ratio of drift current to wind speed, we get the predicted value for amplitude given in Table 4. Again, the measured values are much less.

8. Summary and discussion

Although our data base is limited, we feel that a number of significant results have been achieved:

1) A detection scheme has been devised that uses the energy in a very high frequency band (18–32 Hz) to test for turbulence at the surface.

2) A suitable threshold for breaking events was found.

3) The temporal intermittency for breaking under the given conditions (wind speed 5.9 m s^{-1}, fetch 7 km, dominant wave frequency 0.56 Hz) was found to be 1.2%. The fraction of high-frequency energy (2–32 Hz) in those events was 12%.

4) Under reasonable assumptions, the spatial intermittency and the spatial fractional energy was found to be the same as the temporal quantities.

5) Elevations of the breaking crests were much less than expected. The mean crest height was a

TABLE 4. Amplitude and slope of breaking crests.

	Measured			Expected	
	Mean	Std. dev.	Maximum	L-H*	BP**
All crests:					
Amplitude (cm)	4.4	3.47	17.7	—	—
Slope	0.055	0.044	0.223	—	—
Breaking crests:					
Amplitude (cm)	8.2	3.96	17.7	35.2	33.0
Slope	0.103	0.050	0.223	0.443	0.416

* Longuet-Higgins (1975).
** Banner and Phillips (1974).

quarter of the values predicted by nonlinear studies of steady waves.

Taking the last point first, a number of factors have not been considered in the theoretical comparisons. One is unsteadiness, which is certain to develop due to the Benjamin-Feir (1967) instability. Longuet-Higgins and Cokelet (1978), in numerical calculations, and Melville (1982), in laboratory experiments, have shown that these types of instabilities can lead to wave breaking at somewhat lower values of ak, e.g., for $ak = 0.39$, where this parameter is calculated for an individual breaking crest. This is still much larger than our measured value of 0.1. We did not measure local wavenumber values for the breaking crest; however, we can be quite confident that they are not four times larger than the value calculated using the dispersion relation. In any case, the comparison is not really valid because Longuet-Higgins and Cokelet's calculation and Melville's experiment were for subharmonic interactions, not for wave groups, such as we encountered in the field.

Ochi and Tsai (1983) have studied breaking of irregular waves (typical of sea spectra) in a wave tank without wind. They also found breaking to occur for ak roughly equal to 0.39.

A second factor that we have not considered in comparing to theory is three-dimensional effects. McLean *et al.* (1981) have found that wave trains can be unstable to three-dimensional disturbances for slopes as low as 0.29. This is still three times the measured value.

A third possibility is that the wind plays a more important role in wave breaking than is commonly thought. Schooley (1979) and Okuda *et al.* (1977) have shown that, for small-scale waves under the influence of the wind, the surface drift can vary considerably from crest to trough. Even for large-scale waves, the drift layer, as a viscous flow regime, should respond quickly to variations in surface stress. These variations could be significant, especially if the local boundary flow has separated (Weissman, 1981). The stress would be of such a nature as to increase the drift current near a crest, perhaps to the stage where the particle velocity becomes greater than the crest speed and breaking occurs.

For the measurements on intermittency and fractional energy, very few other measurements have been made with which we can compare our results. In the temporal domain, Longuet-Higgins and Smith (1981) and Thorpe and Humphries (1980) used a wire probe (of unspecified diameter) and a detection algorithm that was based on the rate of change of the elevation signal (which is related to the local slope of the surface). Very few statistics are offered by either of these studies. Under wind conditions similar to ours, Longuet-Higgins and Smith (1981) observed roughly two breaking waves in a 10 minute period. This implies the fraction of breaking events to be 1.3%, whereas we found 8.6% of the crests to be breaking. We can only conclude that their method was not as sensitive as ours to small-scale structures. No information is given on the duration of the events. We can not compare to Thorpe and Humphries' temporal measurements because they did not count individual crests.

The only spatial data available come from photographs of the surface. Whitecap coverage is a measure of spatial intermittency. However, these are actually measurements of the foam that has been produced by wave breaking, not the breaking events themselves. The "small-scale" breaking events (with and without air entrainment) that we can observe with the wire wave gauge are probably not visible in photographs.

Monahan has measured whitecap coverage on lakes (1969) and oceans (1971). His results for similar wind speeds and fresh water are generally a factor of 10 smaller than our estimate of 1.2%.

Thorpe and Humphries (1980) also made spatial measurements. They have calculated N_L/M_L, the number of breaking events as a fraction of total crests. When a wave group had more than one breaking crest, it was only counted once. This was the same as a count of individual breaking crests because it was very rare that they had more than one breaking crest per wave group.[5] For wind speeds similar to our conditions, they found values from 2.5% to 6.5%. These are much closer to our measurements of 8.6%.

In a recent series of papers, Snyder and Kennedy (1983), Kennedy and Snyder (1983) and Snyder *et al.* (1983) have suggested that the vertical acceleration can be used to form a criterion for wave breaking. When vertical acceleration is above a threshold (e.g., 0.5 g), the waves will break. Since we did not measure vertical acceleration, we cannot comment on the validity of this approach. In Section 7, we assume that wave amplitude is used as a threshold, but this

[5] Their temporal group had from one to three individual breaking crests. Note that this is in agreement with our argument of Section 6 that there are twice as many crests per wave group in the temporal domain as in the spatial.

could be any wave parameter. In a "macroscopic" view, amplitude, velocity and acceleration are all related.

We have developed in this study a criterion for the *detection* of wave breaking. Once breaking has started, or just at the onset, we expect increased energy in the very high-frequency components (due to turbulence or a sharp corner in the surface). This cannot be used as a criterion for the *prediction* of wave breaking, but it does give us a definitive means for determining that wave breaking has really occurred.

We anticipate that temporal measurements will continue to be important for some time as our main data source for the true structure of the sea surface. Therefore, the questions raised in Section 6 concerning the conversion of temporal quantities to spatial quantities are very important, such as: "are wave groups evolving slowly?" and "do the breaking events move with the phase speed of the dominant waves?". We hope to address these in the future, along with continued studies of the small-scale structure itself at other wind speeds and fetch.

Acknowledgments. We would like to thank Drs. S. O. McConnell and E. D. Cokelet for their interest, support and lively discussions. Assistance with data collection by Messers. R. J. Lind and R. B. Sunderland is sincerely appreciated. This project was supported by Office of Naval Research Contract N00014-81-K-0095.

REFERENCES

Banner, M. L., and O. M. Phillips, 1974: On the incipient breaking of small scale waves. *J. Fluid Mech.*, **65,** 647–656.

Benjamin, T. B., and J. E. Feir, 1967: The disintegration of wave trains in deep water. Part 1. Theory., *J. Fluid Mech.*, **27,** 417–430.

Evans, D. D., and O. H. Shemdin, 1980: An investigation of modulation of capillary and short gravity waves in the open ocean. *J. Geophys. Res.*, **85,** 5019–5024.

Jones, W. L., and L. C. Schroeder, 1977: Radar backscatter from the ocean: Dependence on surface friction velocity. *Bound. Layer Meteor.*, **13,** 133–149.

Kelvin, L., 1871: Hydrokinetic solutions and observations. Part 3. The influence of wind on waves in water supposed frictionless. *Phil. Mag.*, **4,** 42, 362.

Kennedy, R. M., and R. L. Snyder, 1983: On the formation of whitecaps by a threshold mechanism. Part II: Monte Carlo experiments. *J. Phys. Oceanogr.*, **13,** 1493–1504.

Khalsa, S. J. S., and J. A. Businger, 1977: The drag coefficient as determined by the dissipation method and its relation to intermittent convection in the surface layer. *Bound. Layer Meteor.*, **12,** 273–297.

Kraus, E. B., 1972: *Atmosphere–Ocean Interaction,* Clarendon Press, 275 pp.

Krishen, K., 1971: Correlation of radar backscattering cross section with ocean wave height and wind velocity. *J. Geophys. Res.*, **76,** 6528.

Lake, B. M., and H. C. Yuen, 1978: A new model for nonlinear wind waves. Part 1: Physical model and experimental evidence. *J. Fluid Mech.*, **83,** 49–74.

Liu, H. T., K. B. Katsaros and M. A. Weissman, 1982: Dynamic response of thin-wire wave gauges. *J. Geophys. Res.*, **87,** 5686–5698.

Longuet-Higgins, M. S., 1975: Integral properties of periodic waves of finite amplitude. *Proc. Roy. Soc. London,* **A342,** 157–174.

——, and E. D. Cokelet, 1978: The deformation of steep surface waves on water. II. Growth of normal-mode instabilities. *Proc. Roy. Soc. London,* **A364,** 1–28.

——, and N. D. Smith, 1981: Measurements of breaking waves by a surface jump-meter. Presented at AGU West Coast Meeting, San Francisco. Submitted to *J. Phys. Oceanogr.*

McConnell, S. O., S. S. Atakturk and K. B. Katsaros, 1984: High frequency acoustic sea surface scatter correlated with wind stress and wave height measurements. In preparation (to be submitted to *J. Acoust. Soc. Am.*).

McLean, J. W., Y. C. Ma, D. U. Martin, P. G. Saffman and H. C. Yuen, 1981: Three-dimensional instability of finite-amplitude water waves. *Phys. Rev. Lett.*, **46,** 817–820.

Melville, W. K., 1982: The instability and breaking of deep-water waves. *J. Fluid Mech.*, **115,** 165–185.

Miles, J. W., 1957: On the generation of surface waves by shear flows. *J. Fluid Mech.*, **3,** 185–204.

Monahan, E. C., 1969: Fresh water whitecaps. *J. Atmos. Sci.*, **26,** 1026–1029.

——, 1971: Ocean whitecaps. *J. Phys. Oceanogr.*, **1,** 139–144.

Ochi, M. K., and C. H. Tsai, 1983: Prediction of occurrence of breaking waves in deep water. *J. Phys. Oceanogr.*, **13,** 2008–2019.

Okuda, K., S. Kawai and Y. Toba, 1977: Measurements of skin friction distribution along the surface of wind waves. *J. Oceanogr. Soc. Japan,* **33,** 190–198.

Phillips, O. M., 1980: The dispersion of short wavelets in the presence of a dominant long wave. *J. Fluid Mech.*, **107,** 465–485.

Pond, S., and W. G. Large, 1978: A system for remote measurements of air–sea fluxes of momentum, heat, and moisture during moderate to storm winds. Manuscript Rep. No. 32, Institute of Oceanography, University of British Columbia, Vancouver, B.C., Canada.

Reece, A. M. Jr., 1978: Modulation of short waves by long waves. *Bound. Layer Meteor.*, **13,** 203–214.

Richter, K., and W. Rosenthal, 1981: Energy distribution of waves above 1 Hz on long wind waves. *Proc. IUCRM Symp. on Wave Dynamics and Radio Probing of the Ocean Surface,* Miami, (to be published).

Schlichting, H., 1968: *Boundary Layer Theory,* 6th ed. McGraw-Hill, 740 pp.

Schooley, A. H., 1979: Lagrangian wind and current vectors very close to a short-fetch wind-swept surface. *J. Phys. Oceanogr.*, 1060–1063.

Sinitsyn, Y. A., I. A. Leykin and A. D. Rozenberg, 1973: The space-time characteristics of ripple in the presence of long waves. *Atmos. Ocean. Phys.*, **9,** 511–519.

Snyder, R. L., and R. M. Kennedy, 1983: On the formation of whitecaps by a threshold mechanism. Part I: Basic formalism. *J. Phys. Oceanogr.*, **13,** 1482–1492.

——, L. Smith and R. M. Kennedy, 1983: On the formation of whitecaps by a threshold mechanism. Part III: Field experiment and comparison with theory. *J. Phys. Oceanogr.*, **13,** 1505–1518.

Stolte, S., 1979: Ein modell des kurzwelligen Seegangs im spektralen Frequenzbereich von 0.8 Hz bis 5.0 Hz. *FWG-Bericht 1979–8,* Kiel, 50 pp.

Thorpe, S. A., and P. N. Humphries, 1980: Bubbles and breaking waves. *Nature,* **283,** 463–465.

Weissman, M. A., 1976: A simple model for the generation of ripples. *Mem. Soc. R. Sci. Liege,* **10,** 287–298.

——, 1981: Observation and measurements of air flow over water waves. *Proc. IUCRM Symp. on Wave Dynamics and Radio Probing of the Ocean Surface,* Miami, (to be published).

Wright, J. W., 1966: Backscattering from capillary waves with applications to sea clutter. *IEEE Trans. Antennas Propag.,* **AP-14,** 749–754.